frontiers in Chemistry

ORIGINAL RESEARCH
published: 14 May 2019
doi: 10.3389/fchem.2019.00327

# Ruthenium Picolinate Complex as a Redox Photosensitizer With Wide-Band Absorption

*Yusuke Tamaki, Kazuma Tokuda, Yasuomi Yamazaki†, Daiki Saito, Yutaro Ueda and Osamu Ishitani**

*Department of Chemistry, Tokyo Institute of Technology, Tokyo, Japan*

Ruthenium(II) picolinate complex, $[Ru(dmb)_2(pic)]^+$ (**Ru(pic)**; dmb = 4,4′-dimethyl-2,2′-bipyridine; Hpic = picolinic acid) was newly synthesized as a potential redox photosensitizer with a wider wavelength range of visible-light absorption compared with $[Ru(N^N)_3]^{2+}$ (N^N = diimine ligand), which is the most widely used redox photosensitizer. Based on our investigation of its photophysical and electrochemical properties, **Ru(pic)** was found to display certain advantageous characteristics of wide-band absorption of visible light ($\lambda_{abs} < 670$ nm) and stronger reduction ability in a one-electron reduced state ($E^{red}_{1/2} = -1.86$ V vs. $Ag/AgNO_3$), which should function favorably in photon-absorption and electron transfer to the catalyst, respectively. Performing photocatalysis using **Ru(pic)** as a redox photosensitizer combined with a Re(I) catalyst reduced $CO_2$ to CO under red-light irradiation ($\lambda_{ex} > 600$ nm). $TON_{CO}$ reached 235 and $\Phi_{CO}$ was 8.0%. Under these conditions, $[Ru(dmb)_3]^{2+}$ (**Ru(dmb)**) is not capable of working as a redox photosensitizer because it does not absorb light at $\lambda > 560$ nm. Even in irradiation conditions where both **Ru(pic)** and **Ru(dmb)** absorb light ($\lambda_{ex} > 500$ nm), using **Ru(pic)** demonstrated faster CO formation ($TOF_{CO} = 6.7$ min$^{-1}$) and larger $TON_{CO}$ (2347) than **Ru(dmb)** ($TOF_{CO} = 3.6$ min$^{-1}$; $TON_{CO} = 2100$). These results indicate that **Ru(pic)** is a superior redox photosensitizer over a wider wavelength range of visible-light absorption.

**Keywords: redox photosensitizer, $CO_2$ reduction, photocatalyst, Ruthenium(II) complex, wide-band absorption**

OPEN ACCESS

***Edited by:***
*Hitoshi Ishida,*
*Kitasato University, Japan*

***Reviewed by:***
*Wee Han Ang,*
*École Polytechnique Fédérale de Lausanne, Switzerland*
*Mahmut Özacar,*
*Sakarya University, Turkey*

****Correspondence:***
*Osamu Ishitani*
*ishitani@chem.titech.ac.jp*

***†Present Address:***
*Department of Materials and Life Science,*
*Seikei University, Tokyo, Japan*

***Specialty section:***
*This article was submitted to Inorganic Chemistry, a section of the journal Frontiers in Chemistry*

***Received:*** *30 January 2019*
***Accepted:*** *24 April 2019*
***Published:*** *14 May 2019*

***Citation:***
*Tamaki Y, Tokuda K, Yamazaki Y, Saito D, Ueda Y and Ishitani O (2019) Ruthenium Picolinate Complex as a Redox Photosensitizer With Wide-Band Absorption. Front. Chem. 7:327. doi: 10.3389/fchem.2019.00327*

## INTRODUCTION

Redox photosensitizers, which absorb visible light and facilitate the electron transfer process, play a key role in various photochemical reactions, such as $CO_2$ reduction (Takeda et al., 2017; Tamaki and Ishitani, 2017), water oxidation (Fukuzumi et al., 2016), hydrogen evolution (Schulz et al., 2012), and organic synthesis (Prier et al., 2013). Effective photosensitizers should be endowed with three important properties, including (1) visible-light absorption, (2) a long lifetime in the excited state to initiate the electron transfer process, and (3) reducing and/or oxidizing power that is strong enough to donate electrons or holes to the catalyst. In particular, the utilization of visible-light over a wider range of wavelengths is important both to utilize sunlight efficiently and avoid the internal filter effect and side reactions that are commonly caused by the light-absorption of catalysts and/or electron donor/acceptor. Ru(II) complexes coordinated with three diimine ligands, $[Ru(N^N)_3]^{2+}$ (N^N = diimine ligand) are the most widely used redox photosensitizers in various photochemical

redox reactions because these types of complexes exhibit strong absorption in the visible-light region and have a long lifetime in their triplet metal-to-ligand charge-transfer ($^3$MLCT) excited states (Juris et al., 1988; Thompson et al., 2013).

However, one of the disadvantages of $[Ru(N^{\wedge}N)_3]^{2+}$-type photosensitizers is the limited access to the wavelength region of visible light, e.g., $\lambda_{abs} < 560$ nm in the cases of N^N = 2,2′-bipyridine (bpy) and 4,4′-dimethyl-2,2′-bipyridine (dmb), and these complexes cannot utilize visible light having lower energy ($\lambda > 560$ nm). To overcome this, ligand-modified Ru(II) photosensitizers have been reported. For example, Ru(II) complexes have an extended π-system for photodynamic therapy (Zhang et al., 2017) and multinuclear Ru(II) complexes by conjugated bridging ligand are used for hydrogen evolution (Tsuji et al., 2018). However, these modifications lower the reducing power of photosensitizers and limit the choice of catalyst especially for the reduction of $CO_2$. On the other hand, we have reported an osmium(II) analog, i.e., $[Os(N^{\wedge}N)_3]^{2+}$, which could function as a redox photosensitizer utilizing a much wider wavelength range of visible light ($\lambda_{abs} < 700$ nm) due to its singlet-to-triplet direct excitation (S-T absorption) and drive photocatalytic $CO_2$ reduction by red-light irradiation ($\lambda_{ex} > 620$ nm) in the combination with rhenium(I) catalyst unit (Tamaki et al., 2013b), whereas the high toxicity of $Os^{VIII}O_4$ inhibits the wider application of osmium complexes.

Therefore, we developed a novel ruthenium(II) redox photosensitizer that can utilize a wider wavelength range of visible light than $[Ru(N^{\wedge}N)_3]^{2+}$. In the photocatalytic system for $CO_2$ reduction, a photosensitizer mediates an electron from a sacrificial electron donor to a catalyst. Since the positive shift of the LUMO level of redox photosensitizer should limit the choice of a catalyst for reducing $CO_2$, for the expansion of the useable wavelength range, we try to decrease the energy-gap between HOMO and LUMO by the negative shift of the HOMO level, while maintaining the LUMO level. We introduced anionic electron-donating picolinate instead of a diimine ligand into a ruthenium complex (Norrby et al., 1997; Couchman et al., 1998). $[Ru(dmb)_2(pic)]^+$ (**Ru(pic)**; Hpic = picolinic acid) was synthesized, and we investigated its photophysical properties and functions as a redox photosensitizer using $[Ru(dmb)_3]^{2+}$ (**Ru(dmb)**) as a reference redox photosensitizer and $Re(dmb)(CO)_3Br$ (**Re**) as a catalyst for the reduction of $CO_2$ (Hawecker et al., 1983; Gholamkhass et al., 2005; Tamaki et al., 2016). **Chart 1** shows structures and abbreviations of the metal complexes used.

## RESULTS AND DISCUSSION

**Figure 1** displays UV-vis absorption spectra of **Ru(pic)**, **Ru(dmb),** and **Re** measured in *N*,*N*-dimethylacetamide (DMA). **Ru(pic)** exhibited a broad singlet MLCT absorption band at $\lambda_{abs} = 450$–$640$ nm, with molar absorptivity at an absorption maximum ($\lambda_{max} = 498$ nm) of $1.04 \times 10^4$ $M^{-1}cm^{-1}$, which was red-shifted in wavelength compared to that of **Ru(dmb)** ($\lambda_{abs} = 420$–$550$ nm). The absorption band attributed to the π-π* transition of dmb ligands was observed at 294 nm. According to this result, **Ru(pic)** have the potential to utilize visible light over a wider range of wavelengths ($\lambda_{abs} < 670$ nm) than **Ru(dmb)** ($\lambda_{abs} < 560$ nm). This expected red-shift of the MLCT band should be induced by the stronger electron-donating ability of the picolinate ligand to negatively shift the energy level of HOMO.

**Ru(pic)** exhibited phosphorescence from its $^3$MLCT excited state (**Figure 2**) with a quantum yield of $\Phi_{em} = 0.8\%$ and a lifetime of $\tau_{em} = 66$ ns. Emission spectrum of **Ru(pic)** ($\lambda_{em} = 734$ nm) was also red-shifted compared to that of **Ru(dmb)** ($\lambda_{em} = 638$ nm). The quantum yield and lifetime of **Ru(pic)** were smaller and shorter than those of **Ru(dmb)** ($\Phi_{em} = 9.1\%$, $\tau_{em} = 741$ ns) due to the 12-times faster non-radiative deactivation process (**Ru(pic)**: $k_{nr} = 1.5 \times 10^7$ $s^{-1}$; **Ru(dmb)**: $k_{nr} = 1.2 \times 10^6$ $s^{-1}$), which is a reasonable behavior from energy-gap law. **Table 1** summarizes photophysical properties of **Ru(pic)** along with those of **Ru(dmb)** and **Re**.

**Figure 3** shows the cyclic voltammograms of **Ru(pic)** and **Ru(dmb)** and their redox potentials are summarized in **Table 2** along with that of **Re**. **Ru(pic)** displayed two reversible reduction waves and a reversible oxidation wave, which are attributable to the subsequent reduction of two dmb ligands and the oxidation couple of $Ru^{III/II}$, respectively. Both the first reduction ($E^{red}_{1/2} = -1.86$ V vs. $Ag/AgNO_3$) and oxidation ($E^{0x}_{1/2} = 0.41$ V) waves were observed at more negative potentials than those of **Ru(dmb)** ($E^{red}_{1/2} = -1.74$ V and $E^{0x}_{1/2} = 0.77$ V), which should be induced by the stronger electron-donating ability of the picolinate ligand. The stronger reducing power of one-electron reduced species


**Chart 1 |** Structures and abbreviations of complexes used.

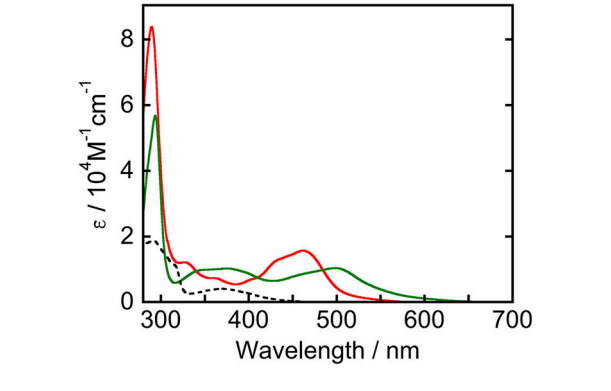


**FIGURE 1 |** UV-vis absorption spectra of **Ru(pic)** (green line), **Ru(dmb)** (red line), and **Re** (broken line) measured in a DMA solution.

(OERS) of **Ru(pic)** ($E^{red}_{1/2} = -1.86$ V) facilitates an increase in the number of choices of applicable catalyst because the electron transfer from OERS of **Ru(pic)** to a catalyst must occur during photocatalysis in the case of reductive quenching mechanisms. When using **Ru(pic)** as a photosensitizer and **Re** as a catalyst, the electron transfer process from OERS of **Ru(pic)** to **Re** ($E^{red}_{1/2} = -1.76$ V) occurs exothermically.

These results indicated that **Ru(pic)** had some advantages with respect to its function as a redox photosensitizer compared with **Ru(dmb)**, including its wider wavelength range of visible-light absorption and stronger reducing power of OERS, which is effective in the electron transfer to the catalyst. However, certain unfavorable properties were also observed, i.e., a shorter lifetime ($\tau_{em} = 66$ ns) and weaker oxidizing power in its excited state ($\Delta E = E$(**Ru(dmb)**$^*$/**Ru(dmb)**$^-$)–$E$(**Ru(pic)**$^*$/**Ru(pic)**$^-$) = 0.28–(−0.11) = 0.39 V). In the reductive quenching process, an excited photosensitizer accepts an electron from a sacrificial electron donor. Weaker oxidation power in the excited state of a photosensitizer should decrease the driving force of this electron transfer process. In addition, since this process competes with the radiative and non-radiative deactivation processes from the excited state of a photosensitizer by itself, the shorter lifetime results in less opportunity of the reductive quenching process to occur. To evaluate whether reductive quenching occurs, the emission intensity from **Ru(pic)** was compared in the presence of five different concentrations of a sacrificial electron donor, 1,3-dimethyl-2-phenyl-2,3-dihydro-1*H*-benzo[*d*]imidazole (BIH) (Tamaki et al., 2013a; Hasegawa et al., 2015) in DMA-triethanoamine (TEOA; 5:1 v/v). As shown in **Figure 4**, the emission intensities from the $^3$MLCT excited state of **Ru(pic)** decreased at higher concentrations of BIH, which indicated that the excited **Ru(pic)** was quenched by BIH. The quenching rate constant was determined to be $k_q = 1.7 \times 10^8$ $M^{-1}s^{-1}$ from the Stern-Volmer plot (**Figure S1**) and the lifetime of the emission ($\tau_{em} = 66$ ns), which was 8-times slower than that of **Ru(dmb)** ($k_q = 1.4 \times 10^9$ $M^{-1}s^{-1}$) as expected from the weaker oxidizing power in the $^3$MLCT excited state of **Ru(pic)**. In the photocatalytic reaction condition, i.e., [BIH] = 0.2 M, 69% of the excited **Ru(pic)** was estimated to be quenched by BIH, which should be enough to initiate a photocatalytic reaction.

To clarify the produced species as a result of the quenching of excited **Ru(pic)** by BIH, UV-vis absorption spectral change was observed during photo-irradiation of **Ru(pic)** in the presence of BIH (**Figure 5**). Irradiation by light at $\lambda_{ex} = 480$ nm caused spectral changes and new absorption bands appeared at $\lambda_{abs} = 420$ and 547 nm. The shape of differential absorption spectra before and after irradiation (**Figure 5B**) were quite similar to that of OERS of **Ru(pic)** obtained by electrochemical spectroscopy (**Figure S2**). These results indicate that the reductive quenching

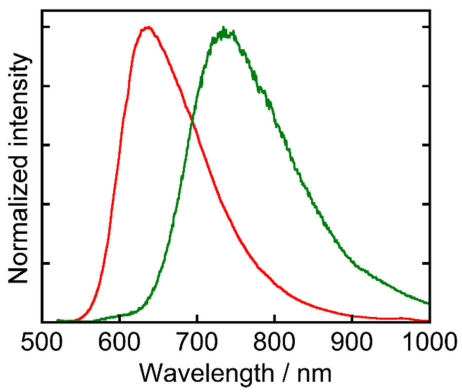


**FIGURE 2 |** Normalized emission spectra of **Ru(pic)** (green line) and **Ru(dmb)** (red line) measured in a DMA solution. The excitation wavelength was 480 nm.

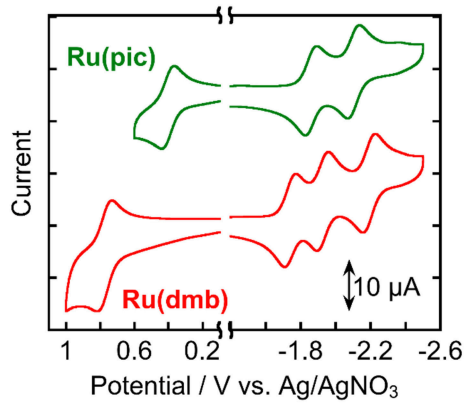


**FIGURE 3 |** Cyclic voltammograms of **Ru(pic)** and **Ru(dmb)** measured in a DMA solution containing $Et_4NBF_4$ (0.1 M) as a supporting electrolyte with a $Ag/AgNO_3$ (10 mM) reference electrode.

**TABLE 1 |** Photophysical properties of **Ru(pic)**, **Ru(dmb)**, and **Re**.[a].

| Complex | $\lambda_{abs}$/nm ($\varepsilon/10^4 M^{-1}cm^{-1}$) | | $\lambda_{em}$[b]/nm | $\Phi_{em}$[b] | $\tau_{em}$[c]/ns | $k_r$[d]/$10^5 s^{-1}$ | $k_{nr}$[e]/$10^6 s^{-1}$ | $E_{00}$[f]/eV |
|---|---|---|---|---|---|---|---|---|
| | $\pi$-$\pi^*$ | $^1$MLCT | | | | | | |
| **Ru(pic)** | 294 (5.67) | 498 (1.04) | 734 | 0.008 | 66 | 1.2 | 15 | 1.75 |
| **Ru(dmb)** | 290 (8.38) | 462 (1.57) | 638 | 0.091 | 741 | 1.2 | 1.2 | 2.02 |
| **Re** | 292 (1.87) | 370 (0.41) | – | – | – | – | – | – |

[a]*Measured in DMA.* [b]*Excitation wavelength: 480 nm.* [c]*Excitation wavelength: 510 nm.* [d]*Rate constants for radiative deactivation calculated as* $k_r = \Phi_{em}/\tau_{em}$. [e]*Rate constants for non-radiative deactivation calculated as* $k_{nr} = (1-\Phi_{em})/\tau_{em}$. [f]*Energy for 0-0 transition obtained from Franck-Condon analyses of the emission spectra.*

**TABLE 2 |** Electrochemical properties of the metal complexes in DMA[a].

| Complex | $E_{1/2}$/V vs. Ag/$AgNO_3$ ($\Delta E$/mV) | | | | $E(PS^+/PS^*)^b$ / V | $E(PS^*/PS^-)^b$ / V |
|---|---|---|---|---|---|---|
| | $Ru^{III/II}$ | M(N^N/N^N·$^-$) (M = Ru or Re) | | | | |
| **Ru(pic)** | +0.41 (72) | −1.86 (72) | −2.11 (69) | – | −1.34 | −0.11 |
| **Ru(dmb)** | +0.77 (68) | −1.74 (72) | −1.93 (70) | −2.19 (74) | −1.25 | +0.28 |
| **Re** | – | −1.76 (74) | – | – | – | – |

[a]*Measured in a DMA solution containing the complex (0.5 mM) and $Et_4NBF_4$ (0.1 M) with a scan rate of 200 mV·s$^{-1}$ under an Ar atmosphere.* [b]*Redox potentials of the photosensitizers (PS) in their excited states were calculated from $E^{0x}_{1/2}$-$E_{00}$ and $E^{red}_{1/2} + E_{00}$, respectively.*

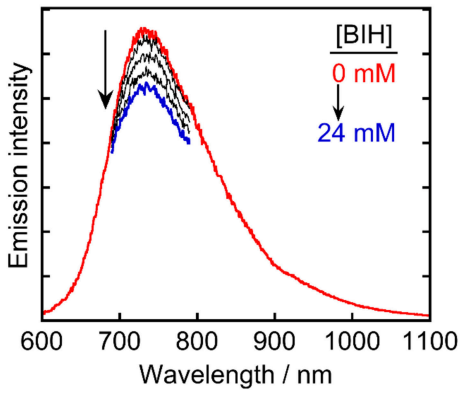


**FIGURE 4 |** Emission spectra of **Ru(pic)** in Ar-saturated DMA-TEOA (5:1 v/v) containing five different concentrations of BIH (0–24 mm).

of the $^3$MLCT excited state of **Ru(pic)** by BIH proceeded successfully to give OERS of **Ru(pic)** (Equation 1) and **Ru(pic)** can be expected to function as a redox photosensitizer over the wide-range absorption of visible light.

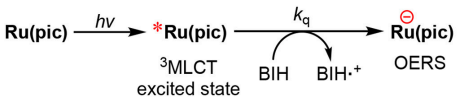


(1)

The results of photocatalytic reactions for the reduction of $CO_2$ are summarized in **Table 3**. In a typical run of photocatalytic reactions, a mixed solution of DMA-TEOA (5:1 v/v) containing **Ru(pic)** (50 μM), **Re** (50 μM), and BIH (0.2 M) as a sacrificial electron donor was irradiated under a $CO_2$ atmosphere using light at $\lambda_{ex}$ > 620 nm. CO production proceeded linearly and selectively and the turnover number for CO production ($TON_{CO}$) was 235 after 36 h of irradiation (**Figure 6A**). The quantum yield for CO formation ($\Phi_{CO}$) was determined to be $\Phi_{CO}$ = 8% using $\lambda_{ex}$ = 600-nm light (light intensity: 6.0 × 10$^{-9}$ einstein·s$^{-1}$). By contrast, when using **Ru(dmb)** as a redox photosensitizer instead of **Ru(pic)**, no photocatalysis proceeded (**Figure 6A**) because **Ru(dmb)** does not absorb lower-energy light at $\lambda_{ex}$ > 620 nm (**Figure 1**). To compare the function as a redox photosensitizer, the photocatalytic reactions were also conducted under photo-irradiation condition, where both **Ru(pic)** and **Ru(dmb)** absorb incident light ($\lambda_{ex}$ > 480 nm). In this condition, both systems photocatalytically produced CO with high selectivity. **Figure 6B** shows the time course of photocatalytic CO production using light at $\lambda_{ex}$ > 500 nm, and the system using **Ru(pic)** formed CO faster ($TOF_{CO}$ = 6.7 min$^{-1}$) than **Ru(dmb)** ($TOF_{CO}$ = 3.6 min$^{-1}$) in the initial stage of photocatalysis. $TON_{CO}$ reached 2347 and 2100 after 36 h of irradiation using **Ru(pic)** and **Ru(dmb)**, respectively. The values of $\Phi_{CO}$ using light at $\lambda_{ex}$ = 480 nm (light intensity: 6.0 × 10$^{-9}$ einstein·s$^{-1}$) were 10% and 44% in the cases using **Ru(pic)** and **Ru(dmb)**, respectively. The **Ru(pic)** system demonstrated similar $\Phi_{CO}$ values in both irradiation conditions ($\lambda_{ex}$ = 600 and 480 nm). These results indicated that **Ru(pic)** has a clear advantage of a wider wavelength range of utilizable visible light compared to **Ru(dmb)**, even for the photocatalytic condition of $\lambda_{ex}$ > 480 nm. Since **Ru(pic)** displays larger molar absorptivity in the $\lambda_{abs}$ > 480-nm region and a wider wavelength range than **Ru(dmb)** (**Figure 1**), **Ru(pic)** absorbs a much larger number of photons at $\lambda_{ex}$ > 480-nm, which leads to a faster $TOF_{CO}$ and larger $TON_{CO}$, even though the quantum yields for CO production were lower.

The quantitative analyses of BIH and its oxidized compound during photocatalysis were conducted in the system using 0.1 M of BIH to simplify the HPLC analyses. As the only oxidized compound of BIH, two-electron oxidized and deprotonated BIH ($BI^+$) was observed (Equation 2).

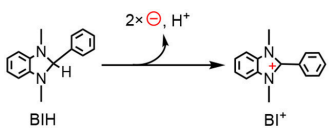


(2)

**Figure 7** shows the change in the amounts of both BIH and $BI^+$ during photocatalytic reaction along with the amount of CO produced. The amount of produced $BI^+$ was fairly similar to that of CO. For example, after 20 h of irradiation, 205 μmol of $BI^+$ and 203 μmol of CO formed. CO is the two-electron reduced compound of $CO_2$, and BIH supplies two electrons per molecule to give $BI^+$ as a oxidized form. These results clearly indicate that BIH acted as a two-electron donor in the photocatalytic reactions using **Ru(pic)** as a redox photosensitizer (Equation 3).

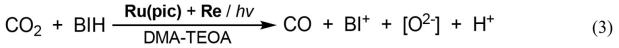


(3)

The reaction mechanisms of the photocatalytic reactions using **Ru(pic)** and **Re** were investigated. Since **Re** does not absorb

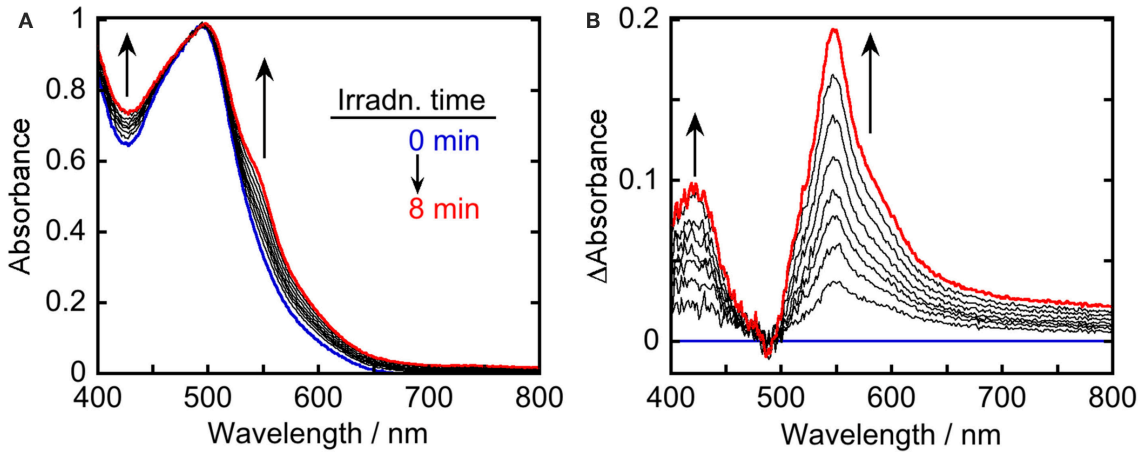


**FIGURE 5 |** UV-vis **(A)** absorption and **(B)** differential absorption spectral change of a DMA-TEOA (5:1 v/v, 4 mL) solution containing **Ru(pic)** (0.1 mM) and BIH (0.2 M) during irradiation using light at $\lambda_{ex} = 480$ nm (0–8 min at 1-min intervals). The incident light intensity was $5.0 \times 10^{-9}$ einstein·s$^{-1}$. Blue and red lines represent spectra at 0 and 8-min irradiation, respectively.

**TABLE 3 |** Photocatalytic properties using the mixed system of the Ru(II) photosensitizer and **Re**[a].

| Photosensitizer | Wavelength | TON[b] | | | $\Phi_{CO}$[f]/% | $k_q$[i] | $\eta_q$[j]/% | $\Phi_{OERS}$[k]/% |
|---|---|---|---|---|---|---|---|---|
| | | CO | HCOOH | $H_2$ | | $10^8$ $M^{-1}s^{-1}$ | | |
| **Ru(pic)** | $\lambda_{ex} > 600$ nm | 235[c] | 4[c] | <1[c] | 8.0[g] | 1.7 | 69 | – |
| **Ru(dmb)** | | n.d.[c,e] | n.d.[c,e] | n.d.[c,e] | – | – | – | – |
| **Ru(pic)** | $\lambda_{ex} > 480$ nm | 2347[d] | < 1[d] | < 1[d] | 10[h] | 1.7 | 69 | 8.3 |
| **Ru(dmb)** | | 2100[d] | 11[d] | < 1[d] | 44[h] | 14 | 99 | 66 |

[a] *A $CO_2$-saturated DMA-TEOA (5:1 v/v) mixed solution containing the photosensitizer (50 μM),* **Re** *(50 μM), and BIH (0.2 M) was irradiated.* [b] *Turnover number for the reaction products after 36 h of irradiation calculated as [product (mol)]/[added* **Re** *(mol)].* [c] $\lambda_{ex} > 620$ *nm.* [d] $\lambda_{ex} > 500$ *nm.* [e] *Irradiation for 12 h.* [f] *Quantum yield of CO production calculated as [CO (mol)]/[absorbed photon (einstein)].* [g] $\lambda_{ex} = 600$ *nm (light intensity: $6.0 \times 10^{-9}$ einstein·s$^{-1}$).* [h] $\lambda_{ex} = 480$ *nm (light intensity: $6.0 \times 10^{-9}$ einstein·s$^{-1}$).* [i] *Quenching rate constants for emission from Ru(II) photosensitizers by BIH obtained from the slopes of Stern-Volmer plots and lifetimes of excited states.* [j] *Quenching fractions of emission from Ru(II) photosensitizers by 0.2 M of BIH calculated as $0.2k_q\tau_{em}/(1 + 0.2k_q\tau_{em})$.* [k] *Quantum yield for one-electron reduction of the photosensitizer using light at $\lambda_{ex} = 480$ nm (light intensity: $5.0 \times 10^{-9}$ einstein·s$^{-1}$).*

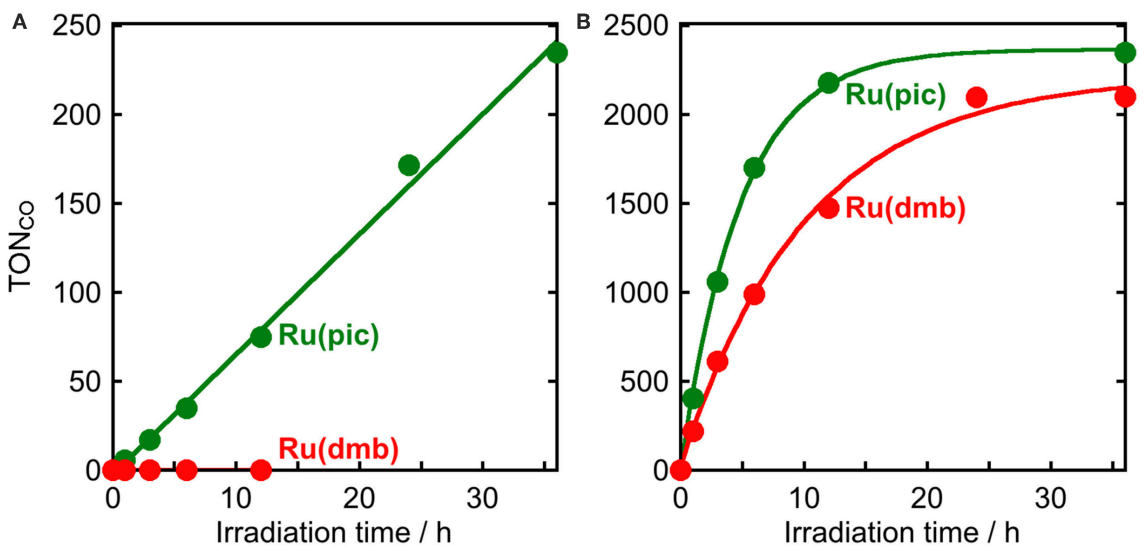


**FIGURE 6 |** Photocatalytic production of CO as a function of irradiation time using **Ru(pic)** (●) or **Ru(dmb)** (●) as a photosensitizer: $CO_2$-saturated DMA-TEOA (5:1 v/v, 2 mL) solutions containing Ru(II) photosensitizer (50 μM), **Re** (50 μM), and BIH (0.2 M) were irradiated at **(A)** $\lambda_{ex} > 620$ nm or **(B)** $\lambda_{ex} > 500$ nm.

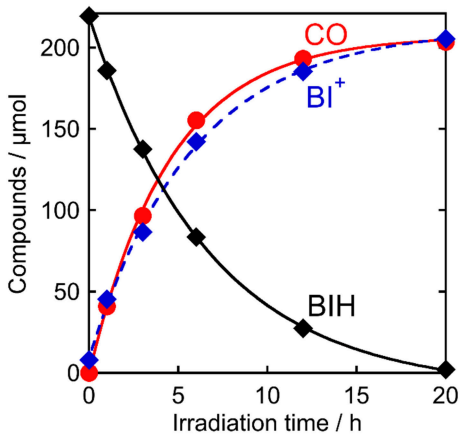


**FIGURE 7 |** Photocatalytic production of CO (●) and $BI^+$ (◆) and consumption of BIH (◆): $CO_2$-saturated DMA-TEOA (5:1 v/v) solutions containing **Ru(pic)** (50 μM), **Re** (50 μM), and BIH (0.1 M) were irradiated at $\lambda_{ex} > 500$ nm.

light at $\lambda_{ex} > 460$ nm, as shown in **Figure 1**, **Ru(pic)** should absorb the irradiated photon selectively under photocatalytic reaction conditions, i.e., $\lambda_{ex} > 600$ nm or $> 480$ nm. The photon absorption by **Ru(pic)** gives its OERS via the reductive quenching process of its $^3$MLCT excited state by BIH, as described above (Equation 1). The reducing power of OERS of **Ru(pic)** ($E^{red}_{1/2} = -1.86$ V) is strong enough to trigger electron transfer to **Re** ($E^{red}_{1/2} = -1.76$ V), which functions as a catalyst for the reduction of $CO_2$. The process of two-electron supply using BIH has already been reported in the photocatalytic reaction system using a Ru(II)-Re(I) supramolecular photocatalyst (Tamaki et al., 2013a). The initial process of the photocatalysis is also a photoinduced electron transfer from BIH to the Ru(II) tris-diimine type photosensitizer unit, forming OERS of the photosensitizer unit and one-electron oxidized BIH ($BIH^{\bullet+}$). $BIH^{\bullet+}$ is rapidly deprotonated by TEOA to give BI•. TEOA functioned only as a base, but not as a sacrificial electron donor to quench the excited photosensitizer unit. BI• has a strong reducing power ($E^{red}_{1/2} = -1.95$ V) (Zhu et al., 2008) enough to provide one more electron to the supramolecular photocatalyst to be converted to $BI^+$. In other words, BIH works as a two-electron donor by one-photon excitation of the photocatalyst via the ECE mechanism. Similar processes should also proceed in the photocatalytic system using **Ru(pic)** and **Re** because both **Ru(pic)** ($E^{red}_{1/2} = -1.86$ V) and **Re** ($E^{red}_{1/2} = -1.76$ V) have a lower reduction potential than BI• ($E^{red}_{1/2} = -1.95$ V). Based on this investigation, the electron-supply processes of BIH are presumed, as depicted in Equation 4.

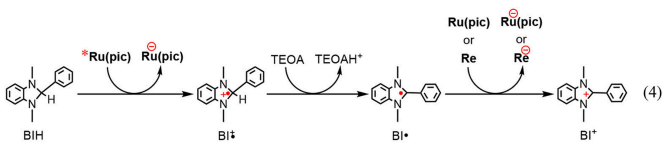


(4)

Photocatalysis using **Ru(pic)** displayed an advantages of a wider wavelength region of visible-light absorption, which achieved both red-light driven $CO_2$ reduction ($\lambda_{ex} > 620$ nm) and faster CO production than the system using **Ru(dmb)** ($\lambda_{ex} > 500$ nm), whereas the quantum yield for CO formation using **Ru(pic)** ($\Phi_{CO} = 10\%$) was 1/4 the value when **Ru(dmb)** ($\Phi_{CO} = 44\%$) was used. The main reason for smaller $\Phi_{CO}$ should be the smaller quantum yield of one-electron reduction ($\Phi_{OERS}$) of **Ru(pic)**. $\Phi_{OERS}$ of **Ru(pic)** using light at $\lambda_{ex} = 480$ nm (light intensity: $5.0 \times 10^{-9}$ einstein·$s^{-1}$) was determined to be 8.3%, which was 1/8 that of **Ru(dmb)** ($\Phi_{OERS} = 66\%$). The elementary processes of one-electron reduction of **Ru(pic)** is displayed in **Scheme 1**. The reductive quenching of the $^3$MLCT excited state of **Ru(pic)** by BIH gives an ion pair, [**Ru(pic)**$^-$···$BIH^{\bullet+}$]. If the ion pair dissociate, free OERS and $BIH^{\bullet+}$ are obtained. The charge-recombination processes from the ion pair or by the re-collision of OERS of **Ru(pic)** and $BIH^{\bullet+}$ should form **Ru(pic)** and BIH. The differences in properties between **Ru(pic)** and **Ru(dmb)**, i.e., the cationic valence and the reducing power of OERS, should affect each elementary process and consequently the quantum yield for one-electron reduction. Since OERS of **Ru(dmb)** is a monovalent cation, the ion pair with $BIH^{\bullet+}$ involves cationic repulsion, which should accelerate the dissociation process. On the other hand, OERS of **Ru(pic)** is zero-valent, which provides no repulsion between $BIH^{\bullet+}$, and therefore, the dissociation process should become slower when using **Ru(pic)** (smaller $k_{esc}$). In addition, since the reducing power of OERS of **Ru(pic)** ($E^{red}_{1/2} = -1.86$ V) is stronger than that of **Ru(dmb)** ($E^{red}_{1/2} = -1.74$ V), the driving forces for the charge-recombination processes become larger when **Ru(pic)** is used (larger $k_{rec1}$, $k_{rec2}$). Consequently, the smaller $\Phi_{OERS}$ using **Ru(pic)** should be induced by the slower dissociation process of the ion pair and the faster charge-recombination processes. The quantitative analyses of the factors controlling $\Phi_{OERS}$ of photosensitizing complexes are in progress and will be reported elsewhere.

In the photocatalytic reaction conditions, the electron-consuming process for $CO_2$ reduction via the electron transfer to **Re** (the broken box in Scheme 1) will compete against the charge-recombination by the re-collision of OERS and $BIH^{\bullet+}$. Therefore, since $\Phi_{OERS}$s were determined in the absence of **Re**, $\Phi_{CO}$ (10%) was larger than the expected value from half of $\Phi_{OERS}$ (8.3/2 = 4.2%), which was derived from the fact that the reduction of $CO_2$ to CO is a two-electron reduction process. Higher reduction potential of **Ru(pic)** should operate in favor of the electron transfer to **Re**. Therefore, the ratio of quantum yields for $CO_2$ reduction between using **Ru(pic)** and **Ru(dmb)**, i.e., $\Phi_{CO}$(**Ru(pic)**)/$\Phi_{CO}$(**Ru(dmb)**) = 10/44 = 0.23, became larger than that for one-electron reduction ($\Phi_{OERS}$(**Ru(pic)**)/$\Phi_{OERS}$(**Ru(dmb)**) = 8.3/66 = 0.13). In other words, **Ru(pic)** has another advantage of faster electron transfer to **Re** in the photocatalysis.

# EXPERIMENTS

## General Procedures

$^1$H NMR spectra were measured using a JEOL ECA400II (400 MHz) system in solutions of acetone-$d_6$. The residual

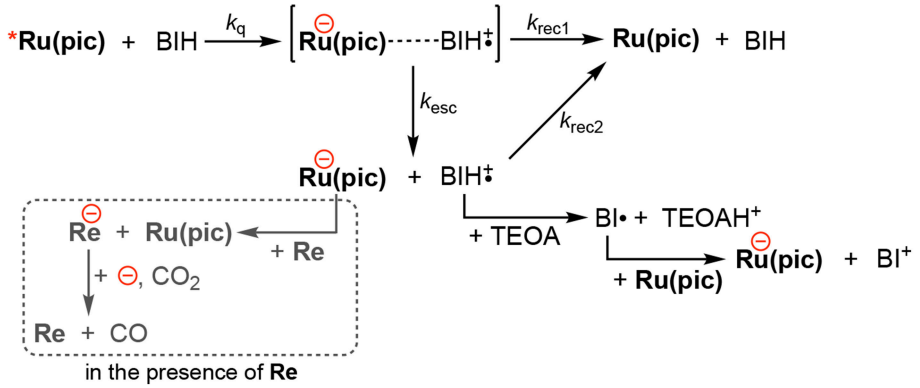


**SCHEME 1 |** The one-electron reduction processes of **Ru(pic)**.

protons of acetone-$d_6$ were used as an internal standard for measurements. Electrospray ionization-mass spectroscopy (ESI-MS) was performed using a Shimadzu LCMS-2010A system with acetonitrile as the mobile phase. UV-vis absorption spectra were measured with a JASCO V-565 spectrophotometer. Emission spectra were measured using a Horiba Fluorolog-3-21 spectrofluorometer equipped with a NIR-PMT R5509-43 near infrared detector. A Horiba FluoroCube time-correlated single-photon counting system was used to obtain emission lifetimes. The excitation light source was a NanoLED-515L pulse lamp (510 nm). A HAMAMATSU absolute PL quantum yield spectrometer C9920-02 was used to determine emission quantum yields. The samples were degassed by Ar-bubbling of solutions for 30 min prior to measuring emissions. Emission quenching experiments were performed on solutions containing the complexes and five different concentrations of BIH. The quenching rate constants $k_q$ were calculated from linear Stern-Volmer plots for the emission from the $^3$MLCT excited state of the photosensitizing complexes and their lifetimes. The redox potentials of the complexes were measured in an Ar-saturated DMA solution containing $Et_4NBF_4$ (0.1 M) as a supporting electrolyte using cyclic voltammetric techniques performed with an ALS CHI-720Dx electrochemical analyzer with a glassy carbon disk working electrode (3 mm diameter), a $Ag/AgNO_3$ (10 mM) reference electrode, and a Pt counter electrode. The supporting electrolyte was dried under vacuum at 100°C for 1 day prior to use. The scan rate was 200 $mV{\cdot}s^{-1}$.

## Photocatalytic Reactions

Photocatalytic reactions were performed in DMA–TEOA (5:1 v/v) solutions containing the photosensitizer (50 μM), **Re** (50 μM), and BIH (0.2 M). After the solution was purged with $CO_2$ for 20 min, the solution was irradiated. For TON measurements, the mixed solution (2 mL) in an 11 mL test tube (i.d. 8 mm) was irradiated in a merry-go-round apparatus using $\lambda_{ex} > 620$ nm light from a halogen lamp equipped with a Rhodamin B (0.2% w/v, $d = 1$ cm) solution filter or $\lambda_{ex} > 500$ nm light from a high-pressure Hg lamp equipped with a uranyl glass and a $K_2CrO_4$ (30% w/w, $d = 1$ cm) solution filter. During irradiation, the temperature of the solution was maintained at 25°C using an EYELA CTP-1000 constant-temperature system. For quantum yield measurements, the mixed solution in a quartz cubic cell (11 mL, light pass length: 1 cm) was irradiated in a Shimadzu photoreaction quantum yield evaluation system QYM-01 using 600 nm or 480 nm light from a 300 W Xe lamp equipped with a 600 nm or 480 nm (FWHM: 10 nm) bandpass filters. The temperature of the solution was controlled during irradiation at 25 ± 0.1°C using an IWAKI CTS-134A constant-temperature system. The gaseous products of photocatalysis, i.e., CO and $H_2$, were analyzed by GC-TCD (GL science GC323). A capillary electrophoresis system (Agilent 7100) was used to analyze HCOOH. HPLC analyses for BIH and $BI^+$ were conducted using a JASCO 880-PU pump, a Develosil ODS-UG-5 column (250 × 4.6 mm), a JASCO 880–51 degasser, and a JASCO UV-2070 detector. The column temperature was maintained at 30°C using a JASCO 860-CO oven. The mobile phase was a 6:4 (v/v) mixture of acetonitrile and a NaOH–$KH_2PO_4$ buffer solution (50 mM, pH 7) with a flow rate of 0.5 $mL{\cdot}min^{-1}$.

## Electrochemical Spectroscopy

Electrochemical spectroscopy to determine the molar absorptivity of OERS was performed using a JASCO PU-980 pump and an EC Frontier flow-type electrolysis cell VF-2 equipped with a carbon felt working electrode (18 mm diameter), a $Ag/AgNO_3$ (10 mM) reference electrode, and a Pt wire counter electrode in an Ar-saturated acetonitrile solution of **Ru(pic)** (0.5 mM) and $Et_4NBF_4$ (0.1 M) as a supporting electrolyte. Applied potential was controlled using an ALS CHI-720Dx electrochemical analyzer and UV-vis absorption spectra were measured using a Photal MCPD-9800 spectrometer (Otsuka Electronics) and a flow-type transmission cell (light pass length: 1.5 mm) (Ishitani et al., 1994).

## Quantum Yields for One-Electron Reduction of Photosensitizers

A 4-mL DMA–TEOA (5:1 v/v) solution of the photosesnsitizer (0.1 mM) and BIH (0.2 M) in a quartz cubic cell (light pass

length: 1 cm) was purged with Ar for 20 min, and then irradiated with the 500-W Xe lamp combined with a 480-nm (FWHM = 10 nm) bandpass filter (Asahi Spectra Co.), ND filter, and a 5-cm-long $H_2O$ solution filter. UV–vis absorption spectral changes during irradiation were measured using a Photal MCPD-9800 spectrometer (Otsuka Electronics). The light intensity was determined as $5.0 \times 10^{-9}$ einstein·$s^{-1}$ using a $K_3Fe(C_2O_4)_3$ actinometer.(Hatchard and Parker, 1956) The amount of OERS of **Ru(pic)** was calculated using the molar absorption coefficient of OERS (500–700 nm) obtained by electrochemical spectroscopy.

## MATERIALS

DMA was dried over molecular sieves 4A, distilled under reduced pressure (∼10 mmHg) and used in a week. TEOA was distilled under reduced pressure (<1 mmHg) and used in a month. Both solvents were kept under Ar in the dark. All other reagents were of reagent-grade quality and used without further purification.

### Synthesis

**Ru(dmb)** (Sullivan et al., 1978), **Re** (Morimoto et al., 2013), and BIH (Hasegawa et al., 2005; Zhu et al., 2008) were prepared according to the methods reported in the literatures. **Ru(pic)** was synthesized using a method similar to the synthesis of $[Ru(bpy)_2(pic)](PF_6)$ (bpy = 2,2′-bipyridine) (Norrby et al., 1997; Couchman et al., 1998), except for using dmb instead of bpy. $[Ru(dmb)_2(pic)](PF_6)$ (**Ru(pic)**): $^1$H NMR (acetone-$d_6$) δ/ppm: 8.81 (d, $J$ = 5.6 Hz, 1H), 8.65 (s, 1H), 8.63 (s, 1H) 8.60 (s, 1H), 8.55 (s, 1H), 8.14 (dd, $J$ = 5.6, 0.8 Hz, 1H), 8.03 (dd, $J$ = 6.4, 2.4 Hz, 1H), 7.94 (d, $J$ = 5.6 Hz, 1H), 7.91 (d, $J$ = 5.6 Hz, 1H), 7.77 (d, $J$ = 5.6 Hz, 1H), 7.70 (dd, $J$ = 5.6, 0.8 Hz, 1H), 7.64 (d, $J$ = 5.6 Hz, 1H), 7.50 (dd, $J$ = 6.4, 2.4 Hz, 1H), 7.43 (dd, $J$ = 5.6, 1.2 Hz, 1H), 7.26 (dd, $J$ = 5.6, 1.2 Hz, 1H), 7.21 (dd, $J$ = 5.6, 1.2 Hz, 1H), 2.67 (s, 3H), 2.58 (s, 3H), 2.55 (s, 3H), 2.49 (s, 3H). ESI-MS (in acetonitrile) m/z: 592 ($[M–PF_6^-]^+$). Anal. calcd for $C_{30}H_{28}F_6N_5O_2PRu·H_2O$: C, 47.75; H, 4.01; N, 9.28. Found: C, 47.72; H, 3.75; N, 9.40.

## CONCLUSION

Ruthenium(II) picolinate complex, **Ru(pic)**, successfully functioned as a redox photosensitizer with a much wider wavelength range of visible-light absorption ($\lambda_{abs} < 670$ nm) compared with a fairly typical **Ru(dmb)** ($\lambda_{abs} < 560$ nm). The system using **Ru(pic)** as a photosensitizer and **Re** as a catalyst photocatalyzed the reduction of $CO_2$ to CO by red-light irradiation ($\lambda_{ex} > 620$ nm). $TON_{CO}$ reached 235 and $\Phi_{CO}$ was 8.0%. Even in the irradiation conditions where **Ru(dmb)** also absorbed light, i.e., $\lambda_{ex} > 500$ nm, the system using **Ru(pic)** demonstrated faster CO formation ($TOF_{CO} = 6.7$ $min^{-1}$) and larger $TON_{CO}$ (2347) than that using **Ru(dmb)** ($TOF_{CO} = 3.6$ $min^{-1}$, $TON_{CO} = 2100$).

## AUTHOR CONTRIBUTIONS

KT, DS, YY, and YT performed all experiments. YU and OI designed this project. YT wrote the manuscript.

## FUNDING

This work was supported by JSPS KAKENHI Grant Numbers JP17H06440 in Scientific Research on Innovative Areas Innovations for Light-Energy Conversion (I4LEC), JP18K14238, JP17K14526.

## SUPPLEMENTARY MATERIAL

The Supplementary Material for this article can be found online at: https://www.frontiersin.org/articles/10.3389/fchem.2019.00327/full#supplementary-material

## REFERENCES

Couchman, S. M., Dominguez-Vera, J. M., Jeffery, J. C., McKee, C. A., Nevitt, S., Pohlman, M., et al. (1998). Structures, electrochemical and spectroscopic properties of ternary ruthenium(II)-polypyridyl complexes with additional carboxylate, biguanide or sulfonamide donors. *Polyhedron* 17, 3541–3550. doi: 10.1016/S0277-5387(98)00145-4

Fukuzumi, S., Jung, J., Yamada, Y., Kojima, T., and Nam, W. (2016). Homogeneous and heterogeneous photocatalytic water oxidation by persulfate. *Chemist. Asian J.* 11, 1138–1150. doi: 10.1002/asia.201501329

Gholamkhass, B., Mametsuka, H., Koike, K., Tanabe, T., Furue, M., and Ishitani, O. (2005). Architecture of supramolecular metal complexes for photocatalytic co2 reduction: ruthenium-rhenium bi- and tetranuclear complexes. *Inorg. Chem.* 44, 2326–2336. doi: 10.1021/ic048779r

Hasegawa, E., Ohta, T., Tsuji, S., Mori, K., Uchida, K., Miura, T., et al. (2015). Aryl-substituted dimethylbenzimidazolines as effective reductants of photoinduced electron transfer reactions. *Tetrahedron* 71, 5494–5505. doi: 10.1016/j.tet.2015.06.071

Hasegawa, E., Seida, T., Chiba, N., Takahashi, T., and Ikeda, H. (2005). Contrastive photoreduction pathways of benzophenones governed by regiospecific deprotonation of imidazoline radical cations and additive effects. *J. Org. Chem.* 70, 9632–9635. doi: 10.1021/jo0514220

Hatchard, C. G., and Parker, C. A. (1956). A new sensitive chemical actinometer. II. Potassium ferrioxalate as a standard chemical actinometer. *Proc. R. Soc. London Ser. A. Mathemat. Phys. Sci.* 235, 518–536. doi: 10.1098/rspa.1956.0102

Hawecker, J., Lehn, J.-M., and Ziessel, R. (1983). Efficient photochemical reduction of CO2 to CO by visible light irradiation of systems containing Re(bipy)(CO)3X or Ru(bipy)32+ -Co2+ combinations as homogeneous catalysts. *J.Chem. Soc. Chem. Commun.* 9, 536–538. doi: 10.1039/c39830000536

Ishitani, O., George, M. W., Ibusuki, T., Johnson, F. P. A., Koike, K., Nozaki, K., et al. (1994). Photophysical behavior of a new co2 reduction catalyst, Re(CO)2(bpy){P(OEt)3}2+. *Inorg. Chem.* 33, 4712–4717.

Juris, A., Balzani, V., Barigelletti, F., Campagna, S., Belser, P., and von Zelewsky, A. (1988). Ru(II) polypyridine complexes: photophysics, photochemistry, eletrochemistry, and chemiluminescence. *Coord. Chem. Rev.* 84, 85–277. doi: 10.1016/0010-8545(88)80032-8

Morimoto, T., Nakajima, T., Sawa, S., Nakanishi, R., Imori, D., and Ishitani, O. (2013). CO2 Capture by a rhenium(I) complex with the aid of triethanolamine. *J. Am. Chem. Soc.* 135, 16825–16828. doi: 10.1021/ja409271s

Norrby, T., Börje, A., Åkermark, B., Hammarström, L., Alsins, J., Lashgari, K., et al. (1997). Synthesis, structure, and photophysical properties of novel ruthenium(II) carboxypyridine type complexes. *Inorg. Chem.* 36, 5850–5858. doi: 10.1021/ic9705812

Prier, C. K., Rankic, D. A., and MacMillan, D. W. (2013). Visible light photoredox catalysis with transition metal complexes: applications in organic synthesis. *Chem. Rev.* 113, 5322–5363. doi: 10.1021/cr300503r

Schulz, M., Karnahl, M., Schwalbe, M., and Vos, J. G. (2012). The role of the bridging ligand in photocatalytic supramolecular assemblies for the reduction of protons and carbon dioxide. *Coordination Chemis. Rev.* 256, 1682–1705. doi: 10.1016/j.ccr.2012.02.016

Sullivan, B. P., Salmon, D. J., and Meyer, T. J. (1978). Mixed phosphine 2,2'-bipyridine complexes of ruthenium. *Inorg. Chem.* 17, 3334–3341. doi: 10.1021/ic50190a006

Takeda, H., Cometto, C., Ishitani, O., and Robert, M. (2017). Electrons, photons, protons and earth-abundant metal complexes for molecular catalysis of CO2 reduction. *ACS Catal.* 7, 70–88. doi: 10.1021/acscatal.6b02181

Tamaki, Y., Imori, D., Morimoto, T., Koike, K., and Ishitani, O. (2016). High catalytic abilities of binuclear rhenium(i) complexes in the photochemical reduction of CO2 with a ruthenium(ii) photosensitiser. *Dalton Trans.* 45, 14668–14677. doi: 10.1039/C6DT00996D

Tamaki, Y., and Ishitani, O. (2017). Supramolecular photocatalysts for the reduction of CO2. *ACS Catal.* 7, 3394–3409. doi: 10.1021/acscatal.7b00440

Tamaki, Y., Koike, K., Morimoto, T., and Ishitani, O. (2013a). Substantial improvement in the efficiency and durability of a photocatalyst for carbon dioxide reduction using a benzoimidazole derivative as an electron donor. *J. Catal.* 304, 22–28. doi: 10.1016/j.jcat.2013.04.002

Tamaki, Y., Koike, K., Morimoto, T., Yamazaki, Y., and Ishitani, O. (2013b). Red-light-driven photocatalytic reduction of CO2 using Os(II)–Re(I) supramolecular complexes. *Inorg. Chem.* 52, 11902–11909. doi: 10.1021/ic4015543

Thompson, D. W., Ito, A., and Meyer, T. J. (2013). [Ru(bpy)3]2+* and other remarkable metal-to-ligand charge transfer (MLCT) excited states. *Pure Applied Chemis.* 85, 1257–1305. doi: 10.1351/pac-con-13-03-04

Tsuji, Y., Yamamoto, K., Yamauchi, K., and Sakai, K. (2018). Near-infrared light-driven hydrogen evolution from water using a polypyridyl triruthenium photosensitizer. *Angew. Chem. Internat. Ed.* 57, 208–212. doi: 10.1002/anie.201708996

Zhang, Y., Zhou, Q., Tian, N., Li, C., and Wang, X. (2017). Ru(II)-Complex-based DNA photocleaver having intense absorption in the phototherapeutic window. *Inorg. Chem.* 56, 1865–1873. doi: 10.1021/acs.inorgchem.6b02459

Zhu, X. Q., Zhang, M. T., Yu, A., Wang, C. H., and Cheng, J. P. (2008). Hydride, hydrogen atom, proton, and electron transfer driving forces of various five-membered heterocyclic organic hydrides and their reaction intermediates in acetonitrile. *J. Am. Chem. Soc.* 130, 2501–2516. doi: 10.1021/ja075523m

**Conflict of Interest Statement:** The authors declare that the research was conducted in the absence of any commercial or financial relationships that could be construed as a potential conflict of interest.